CHALMERS

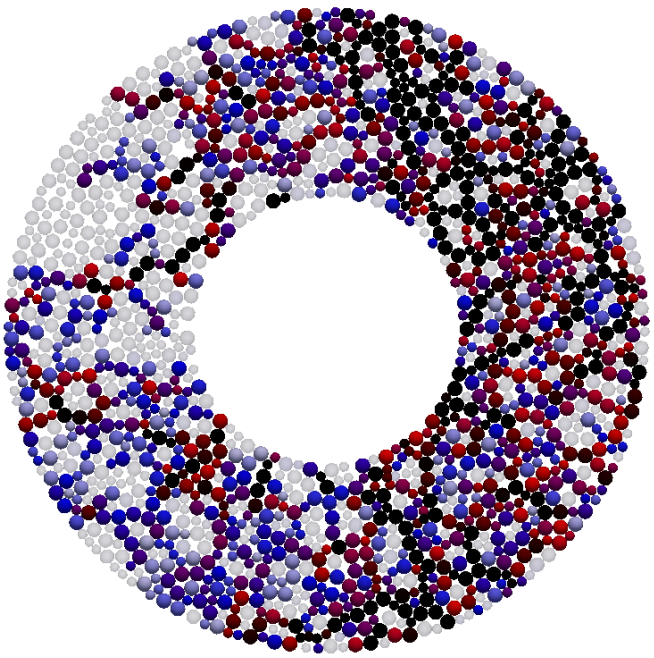

Investigation of stresses in a Couette shear cell using Discrete Element Modeling

Master's thesis in Master program of Applied Mechanics

ADAM JARETEG

Department of Applied Mechanics
Division of Fluid Mechanics
CHALMERS UNIVERSITY OF TECHNOLOGY
Göteborg, Sweden 2014
Master's thesis 2014:63

MASTER'S THESIS IN MASTER PROGRAM OF APPLIED MECHANICS

Investigation of stresses in a Couette shear cell using Discrete Element Modeling

ADAM JARETEG

Department of Applied Mechanics
Division of Fluid Mechanics
CHALMERS UNIVERSITY OF TECHNOLOGY
Göteborg, Sweden 2014

Investigation of stresses in a Couette shear cell using Discrete Element Modeling
ADAM JARETEG

Master's thesis 2014:63
ISSN 1652-8557
Department of Applied Mechanics
Division of Fluid Mechanics
Chalmers University of Technology
SE-412 96 Göteborg
Sweden
Telephone: +46 (0)31-772 1000

Cover:
Figure of particles in a Couette shear cell, colored by stress level.

Chalmers Reproservice
Göteborg, Sweden 2014

Investigation of stresses in a Couette shear cell using Discrete Element Modeling
Master's thesis in Master program of Applied Mechanics
ADAM JARETEG
Department of Applied Mechanics
Division of Fluid Mechanics
Chalmers University of Technology

Abstract

Granular flows are frequently seen in industry today but their complex nature makes it difficult to formulate general macroscopic governing relations. Effort has therefore been given to investigate these flows on detailed microscopic level and from that draw conclusions of the corresponding macroscopic behavior.

In this project, a Discrete Element Modeling (DEM) method is used to simulate dry granular flow in a Couette geometry. The system is dense with particle volume fractions of up to $\alpha = 0.81$. To accurately describe contact forces on the particles a soft-sphere model is used. Macroscopical system stresses are formulated based on the forces on each particle. Shear stresses are evaluated as a function of characteristic properties of the system, including volume fraction, the shear rate and particle friction.

Clear trends on magnitude of the stresses are found for all considered properties. A higher volume fraction, shear rate or friction are shown to result in higher stress levels in the system. Further, tendencies on shear stress related to average normal stress are shown for volume fraction. Where a higher volume fraction results in a relatively lower shear stress.

To investigate the presence of mono sized or of particles of different size in the system, a bimodal distribution of particle sizes is compared to a single size setup. For the distributed particle size calculations the stress magnitude coincide with the single size simulation, whereas the shear to normal stress ratios decrease faster in radial direction from the inner ring.

Keywords: Granular flow, DEM, Couette device

Acknowledgements

I would like to express my gratitude to my supervisor Professor Srdjan Sasic. Thank you for giving me the opportunity to do this thesis and for all the support. Your expertise and advice have been invaluable.

I would also like to express my gratitude to my co-supervisor Klas Jareteg. Thank you for always having the time and the patience to help me. It has been inspiring and exiting to work with you.

Big thanks to the division of Fluid Mechanics for the great company and for providing the coffee necessary for this work.

Finally, thank you Malin for your love and support.

Contents

1 Introduction

1.1 Introduction to granular flows

Flows are conventionally and usually a moving continuous media of some sort. Water and air are maybe the two most common substances and they can both be well described as continuum. But on the microscopic level the flows are small constituents, molecules, of some species with a collective behavior. Granular flows are very similar to the "normal" flows like air and water, but with significantly larger constituents. Sand grains or pellets are two common examples of matter that could make up a granular flow. But the fact that the constituents are roughly the same size as governing length scales of the flow, make certain treatments that works for the "normal" flows a lot harder or impossible to apply for granular flows. One problem is that the stress that arises when formulating the continuum equations for the flow cannot be derived but need to be modeled in some way. For granular flows this is very challenging and it has been a focus for research of the past 20 years.

Figure 1.1: Example of a granular flow

The shear stress in granular flows exhibit different behaviors depending on the shear rate applied [1]. When granulates are subjected to high shear rates, the flow behaves in a similar way to that of gases. While if they are subjected to low shear rates the flow has a solid-like behavior. Shear rates slightly lower than those of the gas-like region can generate a fluid-like behavior and approaching the solid-like region even gives yet another intermediate region. Since granular flows can behave in so many different ways, is it difficult to formulate a general stress model for all regions. To be able to investigate this behavior methods that simulate each particle individually are commonly used in an effort to formulate continuum models.

1.2 The project aim

This project aims to investigate the stresses in a sheared granular flow by studying a semi-two dimensional setup in a geometry called a Couette device. The device consists of an outer and an inner ring (fig. 1.2) with the particles in between. The inner ring rotates at a certain speed inducing a shear to the field of particles. The stresses arising from the shearing can then be calculated and investigated. The particles used in this work are spheres placed in one layer, hence the semi-two dimensionality. Each particle will be treated individually and not as a continuum. Contact forces will be modeled by a soft-sphere model and no interstitial fluid will be present.

The focus of this work is in the investigation of the stresses, i.e. in how the shear rate affects them and how they depend on some characteristic parameters of the system. In this study, the global solid fraction, the particle friction and the particle size distribution are investigated.

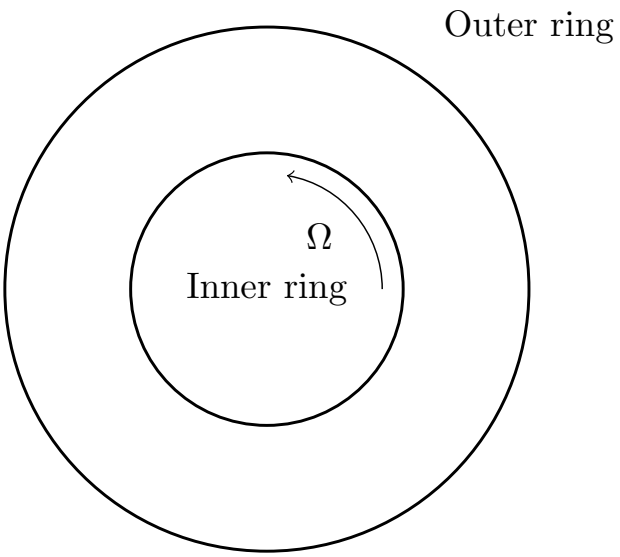

Figure 1.2: A Couette shear cell

A Couette device can be found as a standard research case in many papers (e.g. [2, 3, 4]) for both experiments and simulations. It is therefore beneficial to study that geometry in this project, since it allows for comparisons with previous studies.

2 Theory

When simulating particulates there are two commonly used approaches, or frameworks, the Eulerian one and the Lagrangian one. In the Lagrangian framework each particle in the system is tracked and its motion calculated individually. In contrast, the Eulerian framework views the system of particles as a continuous media and formulates transport equations for mass and momentum in a similar way to those for conventional fluids.

Lagrangian simulations resolve the system in far greater detail compared to the Eulerian methods since each particle is tracked. This means that simulation in the Lagrangian framework can represent more physical phenomena, for example friction or sliding between particles and cohesion. The drawback is long simulation times and, as a consequence, only small systems can be simulated. Eulerian methods are usually faster than the Lagrangian ones and allow for larger systems but have difficulties in correctly capturing complex particle to particle interactions.

2.1 Discrete Element Modeling

Discrete Element Modeling (DEM) is a common Lagrangian simulation approach where each particle is moved according to the Newtons second law of motion

$$m\dot{u} = \sum F \ . \tag{2.1}$$

Where m is mass, u velocity and F are any forces acting on the body. Depending on what forces that are modeled, different interactions can be simulated, based on the same solution method.

The main strategy for resolving the behavior of the particles is to take small steps in time and, for each step, update the position of each particle as calculated by (2.1). This means that for each time step and for each particle one calculates the forces acting on the particle and integrates the acceleration two times to get the position. For this, the algorithm needs to keep track of the previous velocity, position and potential history forces for each particle.

The most common forces in DEM are the contact forces between particles and between particles and walls, together with fluid interaction forces. For the contact forces there are two common groups of models, the hard-sphere and the soft-sphere [5]. The hard-sphere models are used frequently for dilute flows, where the particle interactions are collisional in nature and with only brief contacts. On the other hand, the soft-sphere models are used for dense flows where particle contacts are sustained longer. Depending on application, there are several other forces commonly used in DEM. The gravitational force, cohesional forces and the previously mentioned fluid interaction forces are all frequently used.

The simulation time in DEM depends heavily on which forces are taken into account and how complex those forces are. As an example, when simulating particle-fluid interactions, the fluid flow needs to be resolved to obtain forces acting on the particle and such a calculation can be quite time consuming.

In this project only the gravitational force and the contact forces are considered. The soft-sphere model is used to describe the forces arising from contact between particles and between particles and the walls, since the character of the problem is such that the particles will be under sustained contacts with one another.

2.2 The soft-sphere model

The purpose of the soft-sphere model is to represent the force arising when two bodies are in contact, in this case two spherical particles. Compared to other force representations, the soft sphere model allows for prolonged contacts to be resolved. It also makes possible a detailed description of the friction.

The model detects when two particles are so close to each other that they overlap (fig. 2.1), defined as

$$\xi = (R_A + R_B) - (\bar{r_A} - \bar{r_B}) \ . \tag{2.2}$$

When that happens a repulsive force is introduced as a function of the overlap.

For this project the normal force between two particles is in analogy with a mechanical spring and dashpot system. The force is defined as,

$$F_n = k_n \xi^{\frac{3}{2}} - \eta_n u_{AB} \ . \tag{2.3}$$

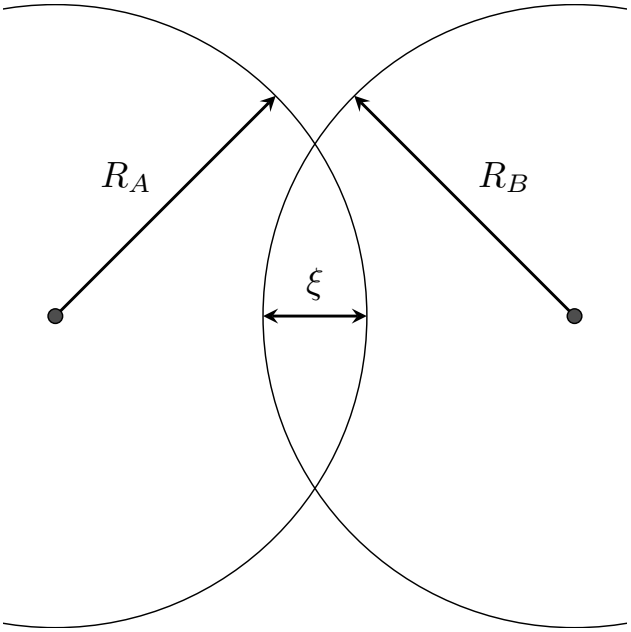

Figure 2.1: Particle overlap

In 2.3, ξ is the normal overlap between the particles (as in equation 2.2), k_n is a spring coefficient related to the material properties of the particles, η_n is a dashpot coefficient controlling energy dissipation and u_{AB} is the relative speed between the two particles.

The first part of the equation (2.3) is the Herz model [6] for colliding spheres and it models the contact itself. The second part of the equation is a dashpot representation for the inelasticity of the contact and it represents the energy loss in the collision. The dashpot term also introduces a certain amount of energy dissipation into the system making the simulations more stable.

For the representation of tangential forces there are two different force formulations depending on if there is sliding between the particles or not. It is calculated as,

$$F_t = \begin{cases} -\mu|F_n|, & \text{for } k_t\xi_t > \mu|F_n| \\ -k_t\xi_t - \eta_n u_{slip}, & \text{else,} \end{cases} \tag{2.4}$$

where, ξ_t is the tangential overlap defined as

$$\xi_t = u_{slip}\Delta_t \ . \tag{2.5}$$

All definitions of coefficients in equations 2.3 and 2.4 are summarized in table 2.1.

Coefficient	Formulation
Normal spring constant	$k_n = \frac{4}{3}\sqrt{R_{eff}}E^*$
Tangential spring constant	$k_t = 8\sqrt{R_{eff}\xi_t}G^*$
Dashpot constant	$\eta_n = \alpha\sqrt{M_{eff}k_n}\xi^{\frac{1}{4}}$
Scaled Young's modulus	$E^* = \frac{E}{2(1-\sqrt{\nu})}$
Scaled shear modulus	$G^* = \frac{G}{2(2-\nu)}$
Shear modulus	$G = \frac{E}{2(1+\nu)}$
Effective mass	$M_{eff} = \frac{M_A M_B}{M_A+M_B}$
Effective radius	$R_{eff} = \frac{d_A d_b}{2(d_a+d_b}$

Table 2.1: Soft-sphere model constants

The soft-sphere model is evaluated each time an overlap between two particles is detected and the model is evaluated once for that pair at each time step. This sets some requirements on the solution algorithm, or more precisely, on the time stepping of the algorithm. If the time steps are too big, the overlaps can become

large each time step. If they do, there is a risk that the forces grows nonphysically large. For each collision there is a theoretical collision time calculated

$$t_n = \pi^{\frac{7}{5}} \left(\frac{5}{4}\right)^{\frac{2}{5}} R \left(\frac{\rho}{E^* \sqrt{|u|}}\right)^{\frac{2}{5}} . \tag{2.6}$$

Where R is the particle radius, u is the particle velocity and $E*$ is a scaled Young's modulus given in table 2.1. It is important to resolve this time in detail to accurately capture the collisional behavior and to limit the overlap.

2.3 Definitions of system quantities

DEM gives thorough description of the system and how it behaves. But to be able to interpret the results of a DEM simulation and compare them to, for example, Eulerian simulations different measurements and quantifications are needed. Since the stresses in the system are modeled in the Eulerian simulations and are needed for any continuous description of the system, they constitute one central quantity. Another important system parameter is the solid fraction, or volume fraction, which describes how much of the entire volume is occupied by the particles.

2.3.1 Stresses in granular flows

To calculate the stresses in granular flow, a method is required to transform forces in contacts between particles into a global field of stresses. One way of doing this is described by Lätzel et al. [2] where

$$\sigma = \frac{1}{V} \int_V dV' \sigma' . \tag{2.7}$$

In (2.7) σ is the stress for an arbitrary volume V and $\sigma' = \sigma'(\mathbf{x})$ is the arbitrary local stress in that volume. In the case of particles, the local stress $\sigma'(\mathbf{x})$ is the stress of a particle at the position $\mathbf{x}$, $\sigma^p(\mathbf{x})$. The integration then reduces to a sum over the particles belonging to the volume,

$$\sigma = \frac{1}{V} \sum_{p \in V} V^p \sigma^p . \tag{2.8}$$

In equation (2.8) the assumption is done that the force f_c of a contact c acting on the particle is constant over the contact surface. An expression for the mean particle stress σ^p can be derived as,

$$\sigma^p = \frac{1}{V^p} \sum_{contacts\ c} f_c \otimes l_c^p . \tag{2.9}$$

Where l_c^p is the vector from the center of the particle p to the point of contact c.

2.3.2 Stress measurements

The stress σ is a tensor but a scalar quantification of it significantly simplifies comparison between cases. In Luding [7] one way of quantifying the deviatoric part of the stress tensor is to take the square root of the second invariant of the stress tensor as,

$$\sigma_D = \sqrt{(\sigma_1 - \sigma_3)^2 + (\sigma_1 - \sigma_2)^2 + (\sigma_2 - \sigma_3)^2}/\sqrt{6} . \tag{2.10}$$

Where σ_{1-3} are the principal stresses. This quantifies the maximum shearing stresses in the system and is related to the common von Mises stress as,

$$\sigma_D = 3\sigma_{vM} . \tag{2.11}$$

Another important measure of the stress tensor is the trace , σ_T, of the tensor. It illustrates the magnitude of the stresses and is defined as,

$$\sigma_T = \sum_{k=1}^{3} \sigma_{kk} \tag{2.12}$$

The trace is also closely related to the averaged normal stresses, or pressure, σ_p as [1],

$$\sigma_T = 3\sigma_p \ . \tag{2.13}$$

2.3.3 Solid fraction

For this project the solid fraction α, often referred to as the volume fraction, is calculated based on the fraction of the total area that the particles occupies as,

$$\alpha = \frac{1}{A^V} \sum_p A^p \ . \tag{2.14}$$

In equation (2.14), A^p is the projection area of the particle p and A^V is the projected area of volume V. Normally the areas in equation (2.14) would be volumes. But the solid fraction can be formulated as (2.14) as a consequence to the two dimensional setup used in this work. The definition of the volume V is changing throughout this project. For clarity will the terms "global solid fraction" or "solid fraction" be used for the solid fraction. Where all the particles projected area will be divided with the entire domains projected area. The term "bin solid fraction" will be used when the particles belonging to a bin is compared to that bin. Noteworthy is also that there exists an upper limit that α can take for packing equally sized circles (area projection of spheres) and it is $\alpha_{max} = 0.9069$.

2.3.4 Shear rate

The shear rate (γ) in the system will have a major impact on the behavior. Depending on the shear rate, the particles can exhibit either gas-like, solid-like or a more undefined intermediate behavior. In the literature there exist a few definitions to the shear rate. One definition used in Luding [7] and applied to the Couette geometry is

$$\gamma = \frac{1}{2}\sqrt{\left(\frac{\partial u_\phi}{\partial r} - \frac{u_\phi}{r}\right)^2 + \left(\frac{\partial u_\phi}{\partial z}\right)^2} \ . \tag{2.15}$$

In equation u_ϕ is the velocity in the tangential direction in a cylindrical coordinate system. This formulation is difficult to use for the shear rate calculation, due to the fact that u_ϕ is a system property that first needs to be estimated from the particles motion. Tardos et al. [1] use an application-oriented definition where

$$\gamma = \frac{\omega R}{H} \ . \tag{2.16}$$

In (2.16), ω is the angular frequency applied to the system, R is the inner ring radius and H is the gap width of the geometry. This formulation is easier to use for the Couette device and it is this definition that is used in the remainder of the project.

3 Methodology

3.1 Simulation method

For this project the open source software OpenFOAM has been used. The software is mainly developed for computational fluid dynamics (CFD) but it has a library for DEM with soft-sphere models. Since it is an open source software, it is straightforward to reuse any existing code for new implementations. The heritage in CFD also enables fluid interactions to be easily added to the simulations. But since the main part of the software is designed for CFD there are also some limitations. The software performs three dimensional simulations. For this project, a two dimensional simulation would have been preferable since the theory is developed for two dimensional setups. The software is also limited to spherical shapes for the DEM simulations. Both limitations can be overcome with new implementations but the problems lie relatively deep in the structure of the code. This makes reimplementations complicated and time consuming.

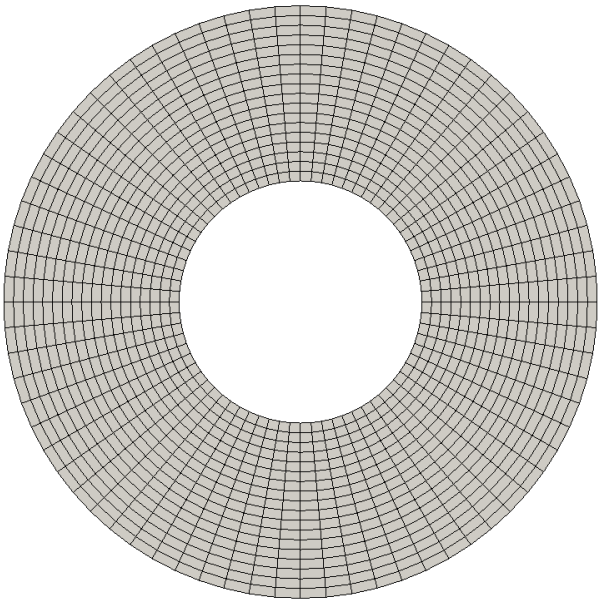

Figure 3.1: Discretization of the Couette geometry

The DEM library uses a significant part of the structure from the CFD core of the software. Some procedures in the simulations are therefore required even though they may not be necessary in the general DEM methodology. The requirement for a mesh is on of such procedures. It is in principal not necessary for DEM simulations to use a mesh but some key functions of OpenFOAM require it. The mesh describes the shape of the geometry (fig 3.1). It also stores some information for the simulations. Each cell in the mesh will store a list with the particles occupied in the cell. Each cell also stores a list with all other cells close enough so that particles belonging to either cell might collide (fig 3.2). This reduces the time consumption for evaluating the particle-particle interactions. The distance two cells need to be apart for no particle-particle collisions to be possible, is referred to as the interaction distance.

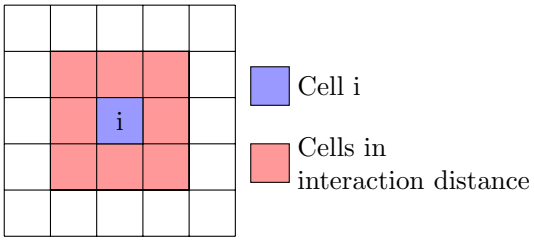

Figure 3.2: Cell interaction distance

3.2 Solution procedure

In the theory section (2.1) a general procedure of DEM simulations was presented. This section aims to describe how that procedure was performed in this project. Even if this project is carried out without an interstitial fluid, it will be briefly mentioned where in the simulations the fluid force would be taken into consideration. This will be done since the simplicity of adding a fluid to the simulations is one of the main strengths in using OpenFOAM to perform DEM calculations.

As mentioned in section 2.1, the solution process takes small steps in time and for each step updates the particle positions. Here, two different time steps are used. One is a collision time step, Δt_{sub}, to accurately resolve contacts. The other is a global time step, Δt_g, that determines the resolution of the other forces (e.g. the fluid forces or the gravitational force).

Each global time step is divided into sub time steps to guarantee that even the fastest collision will still be resolved in sufficient detail. This is done by first calculating the shortest collisional time ($t_{\min}$) possible, calculated as in (2.6), with n_{res} as the number of steps to resolve the collision

$$t_{\text{coll}} = \frac{t_{\min}}{n_{\text{res}}} \ . \tag{3.1}$$

Each sub-time step then becomes,

$$\Delta t_{\text{sub}} = \min(\Delta t_g, t_{\text{coll}}) \ . \tag{3.2}$$

For each sub-time step, the corresponding sub iteration begins with all forces on the particles not due to collision to be calculated and the particle positions updated correspondingly. In this study that was only the gravitational force but this is the step where fluid interaction would be taken into consideration. When the update is completed, all collisional forces are calculated. For each particle, a check is first done on which particles that are located in the possible interaction distance. This is all particles that belong to cells within the interaction distance. For those particles in the possible collision range an overlap check is performed. If an overlap is detected, the corresponding force is calculated using equations (2.3) and (2.4). The particle-wall collisions are evaluated in the same manner, first evaluating potential overlaps, then performing a calculation of the force.

When all collisional forces on all particles are updated, the particle positions are updated and the sub-iteration is completed. To reiterate, in the sub iterations only the movement of the particles are calculated. If there were a fluid present in the system it would only be updated for each global time step Δt_g.

3.3 Stress calculations

To calculate the stresses, as defined in equation (2.8), a spacial discretization of the Couette device is performed. The geometry is divided into a number of radial bins as shown in figure 3.3. In each bin, an average stress value represents the stresses of the particles in that bin. This results in a discretized radial stress profile in the geometry.

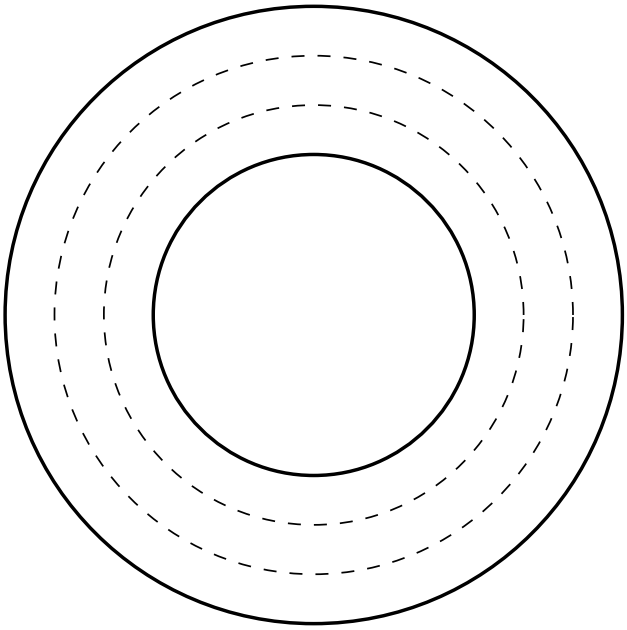

Figure 3.3: Example of bin discretization of the Couette geometry. In this case, three bins are used.

When averaging the stresses in a bin, a particle weighting factor is introduced to compensate for the event that a particle may not be entirely within the bin domain. This is done to reduce the dependence of the averaging volume. Compared to another common averaging technique, where an entire particle is assigned to a bin based on its center, introducing particle weights allows for using narrower bins and, as a consequence, a higher resolution [2].

The weight factor is calculated as in [2],

$$w^p = \frac{A_b^p}{A^p} \ , \tag{3.3}$$

where A_b^p is the area projection of particle p onto the plane of the bin b and is calculated as

$$A_b^p = R^2 \left(\pi - \phi_b + \sin\phi_b \cos\phi_b - \phi_{b+1} + \sin\phi_{b+1} \cos\phi_{b+1}\right) \ . \tag{3.4}$$

The weight is calculated with the approximation that a ring intersects a particle only with straight lines as seen in figure 3.4, where the different angles are defined as $\phi_b = \arccos((r_p - r_b)/R)$ and $\phi_{b+1} = \arccos((r_{b+1} - r_p)/R)$.

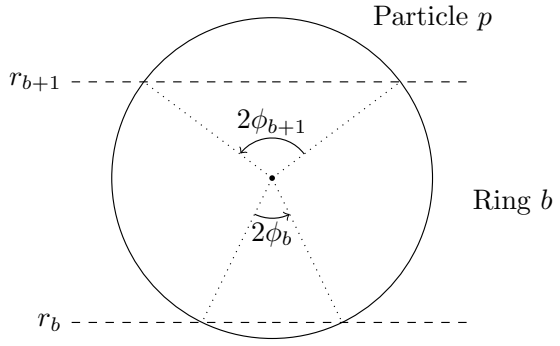

Figure 3.4: Angles for weight calculation

The stress of a single bin, σ_b, then becomes

$$\sigma_b = \frac{1}{V_b} \sum_{p \in V} w_V^p \sigma^p \ . \tag{3.5}$$

The comparison between the deviatoric part and the trace of the stress tensor (σ_D/σ_T), termed the deviatoric fraction, has extensively been used for this study. The deviatoric part of the stress tensor is in a

state of pure shear and the measurement σ_D is closely related to the maximum shear stress observable in the system. The trace of the stress tensor is instead related to the normal stresses. If the trace would be divided by 3, one would obtain what normally is defined as the pressure (eq 2.13). The deviatoric fraction serves as a qualitative measurement of the stresses in the system and describes how large the shear stresses in the system are compared to the average normal stresses. As a comparison with solid mechanics, this would be equivalent to comparing the von Mises stress with the hydrostatic pressure.

Data from the simulation are extracted at user-specified intervals. It is at such points that the stresses are evaluated. At the extraction time, the stress calculations will be based on the contact forces on the particles at that specific moment. This makes the stresses a result of a snapshot in time with no time averaging applied. This fact makes the stresses from one snapshot to another usually very different even if they are close to each other in time.

3.4 Particle initialization

Each simulation the starts with an initial distribution of particles in the geometry. The way this is performed influences the simulations in two ways, *i*) what solid fraction that is achievable and *ii*) what the lattice of particles will be like in the beginning. It is important to point out that, if the particles do not break up from the lattice they are initially placed in, the solution is in fact dependent on the initial state. Previous research done by Veje et al. [8] suggests that the time scales that govern the outer regions are long. This could imply that the simulations need to be run for long durations or that the problem might be dependent on the initial configuration. The problem then emerges that the initialization of the particle field might in fact be a simulation parameter. For this study two different methods for placing the particles have been used to investigate this.

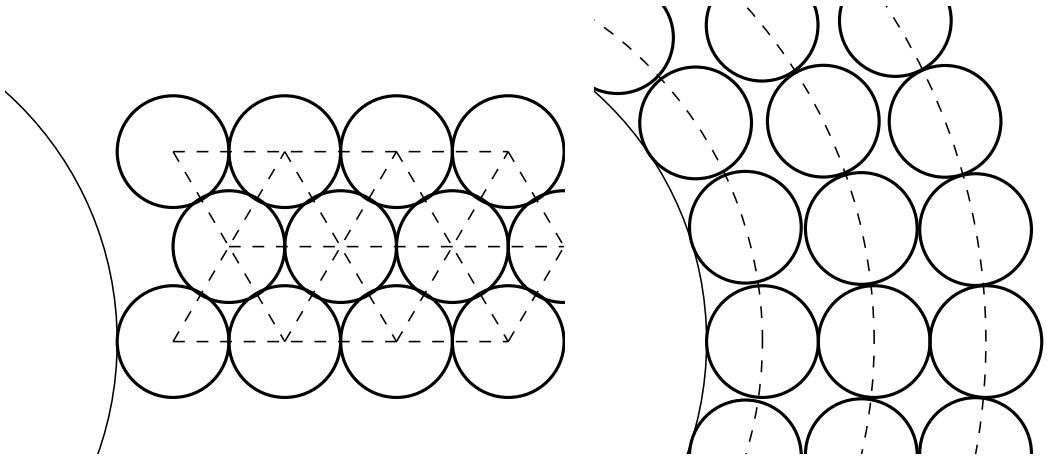

(a) Triangular placement pattern (b) Circular placement pattern

Figure 3.5: The two different initial placement patterns

The first method places the particles in a triangular pattern like the one shown in figure 3.5(a), while the second method initializes the particles in a circular pattern as in figure 3.5(b).

The triangular lattice is the closest packing achievable when packing circles and would theoretically reach solid fractions around $\alpha_{max} \approx 0.9069$. This is not reachable in the simulated geometry since placing particles close to the wall is restricted and it is not possible to perfectly fit the lattice to the circular shape of the geometry. The maximum packing reachable for the cases tried in this project was around $\alpha_{max} \approx 0.85$. The problem with this lattice is that already in the initialization will the particles be placed in a very stiff pattern which does not allow for a natural flow.

The circular placement pattern does not reach as high solid fractions as the triangular pattern does and is, for this application, limited to solid fractions around $\alpha_{max} \approx 0.78$. This limit is fairly low and the majority of the studies in literature [2, 8] investigate higher solid fractions, up to $\alpha \approx 0.82$. The benefit of placing particles in this lattice is that the structure is not as rigid as the triangular one.

Both ways to initialize the particles are based on that the inner and outer ring are perfect circles. Although

the shape in the simulation closely resembles the desired one, it is not exactly circular. The geometry is discretized into a mesh (fig. 3.1) and the walls are constituted of many straight lines instead of a smooth arc. This generally has a minor influence on the simulations but it does make a difference in the very beginning. Due to the straight edges, some particles will be placed partly inside the walls. The solution algorithm will interpret this as an overlap between the wall and the particle and it will result in an added force in accordance with the soft-sphere model. This introduces artificial forces during the initial period of a simulation and it is important not to use the data from such a period.

4 Results and discussion

In this section, the results from the project will be presented and discussed. First will the initial period of the simulations be discussed. Afterwards, a discussion will be given on some system characteristic properties and their impact on stresses in the geometry. Lastly, a section on how the shear rate affects the shear stresses in the system.

The simulations in this study center around a standard case setup. Every test performed has its base in the standard case where the investigated parameters are changed. This allows for an easy comparison between different tests and enables an efficient structure for running the simulations.

In table 4.1, the setup for the standard case is given.

Property	Value
Initial particle placement	Triangular lattice
Simulation time	$t = 10\,\mathrm{s}$
Particle diameter	$d_p = 10\,\mathrm{mm}$
Particle density	$\rho_p = 964\,\frac{\mathrm{kg}}{\mathrm{m}^3}$
Young's modulus of particle	$E_p = 600\,\mathrm{MPa}$
Poissons ratio of particle	$\nu = 0.35$
Angular frequency of inner ring	$\Omega = 10\,\frac{\mathrm{rad}}{\mathrm{s}}$
Particle friction	$\mu = 0.8$
Wall friction (inner/outer ring)	$\mu = 1$
Wall friction (bottom/top)	$\mu = 0.1$
Collision resolution	$n_{res} = 12$
Scaling of viscous damping	$\alpha = 0.12$

Table 4.1: Standard case settings

4.1 Initial setup and convergence

Convergence is achieved when a simulation reaches some sort of a steady state (where residuals are used as measures). The physics of the problem in the present work are such that the forces (and as a result, the stresses) will spontaneously and quickly form and break and a steady state is difficult to define. Still, a convergence check is necessary and for this project that has been an inspection of the development of the deviatoric stresses.

In section 3.4 it was described that in the beginning of the simulations it is likely that artificial forces will appear from the initial placement of the particles. Figure 4.1 shows a typical time development of a moving average of the average deviatoric stress in the domain. In each time step the deviatoric stresses (eq 2.10) in the domain have been averaged and from those values a moving average of the last $0.4s$ is created. The initial time (approximately the first two seconds) of the simulation shows a significantly different behavior than the rest of the simulation which is attributed to the initialization of the problem. To avoid this region of artificial results, all data for analysis are taken after two seconds. That seems to be a common point for most of the simulations where the initial effects are no longer visible.

It has also been investigated if there is any difference in using the two different patterns for particles placement (discussed in sec. 3.4). In figure 4.2, the deviatoric fraction and in figure 4.3, the trace of the stress for the two cases are compared. For both measurements there are differences and the triangular lattice seems to give slightly higher both deviatoric fractions and the trace. This means that, when other parameters are investigated, the same initialization of particles is required to be able to compare the results.

For the other tests performed in this project the triangular pattern is used due to the fact that it allows for higher solid fractions to be simulated. In section 3.4 it was stated that the maximum solid fraction the circular algorithm produces is $\alpha \approx 0.78$, which is considered too low for this study. Solid fractions around $\alpha = 0.81$ are desired here, and they can be produced by the triangular pattern.

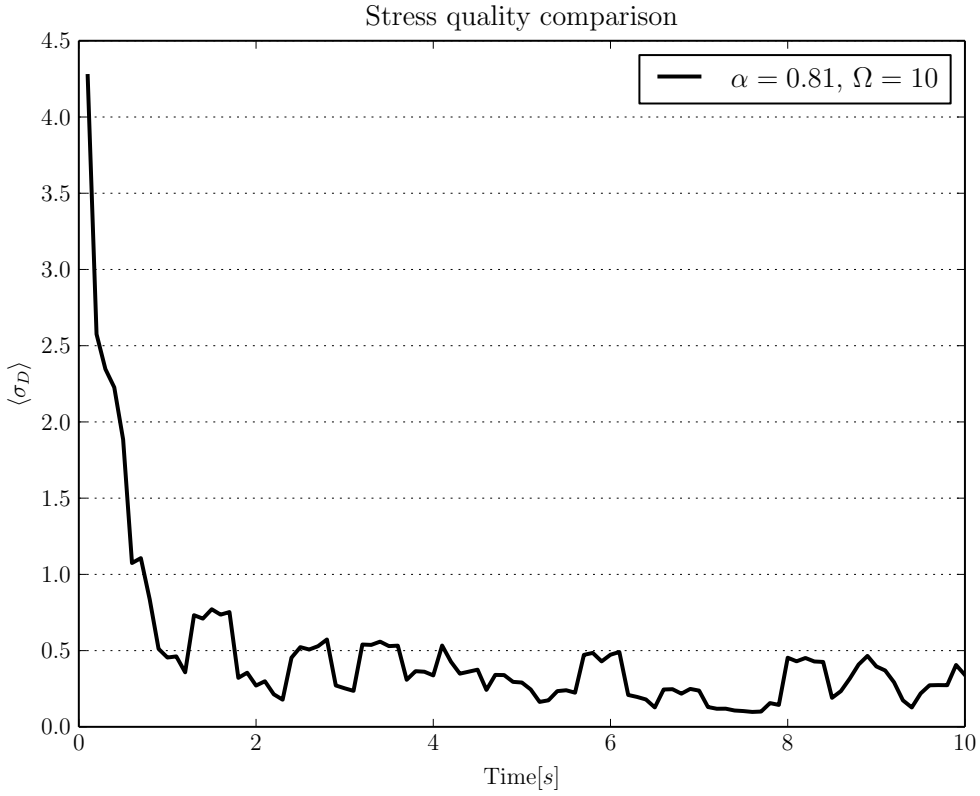

Figure 4.1: Time development of a typical simulation

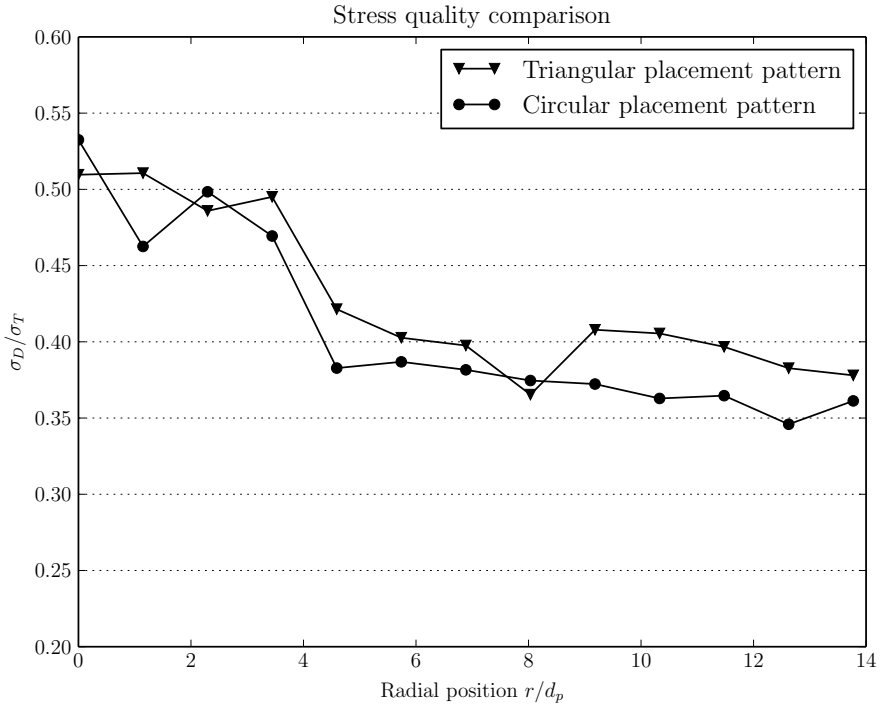

Figure 4.2: The deviatoric fractions for different initial particle placements

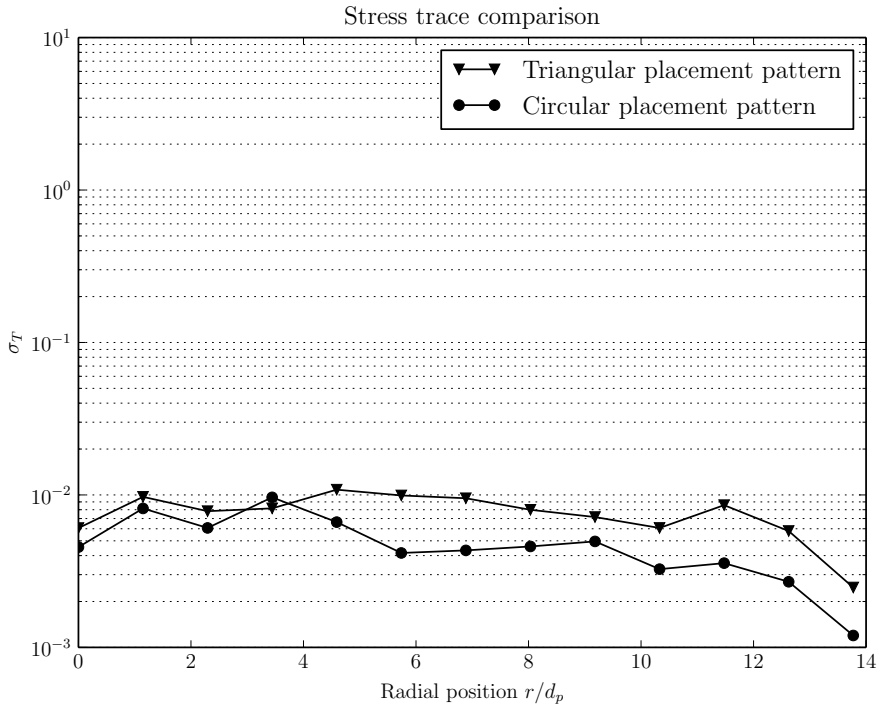

Figure 4.3: The trace of stresses for different initial particle placements

4.2 Parameter study

In this part the results of the parameter studies will be presented. It is investigated how the global solid fraction, particle friction and particle size distribution will affect the stresses in the device.

Focus has been on the two previously mentioned stress measurements, deviatoric stress (sec. 2.3.2 eq. 2.10) and the trace of the stress tensor (sec. 2.3.2 eq. 2.12). Each data point in the graphs to follow represents the averaged stress for a bin (sec. 2.3.1). For the following plots 13 bins have been used for the calculations. The gap width in the Couette cell is around $H \approx 15d_p$ and with 13 bins each bin is larger than the particles. In Lätzel et al. [2] the authors show that using bins lager than the particle size is preferred in order to achieve independence of the averaging volume. The x-axis coordinates have been normalized with the particle diameter (d_p) and translated in such a way so that $x = 0$ is at the inner ring.

4.2.1 Influence of solid fraction

Figure 4.4 shows the deviatoric fraction and figure 4.5 shows the trace of the stress tensor for three different solid fractions, α.

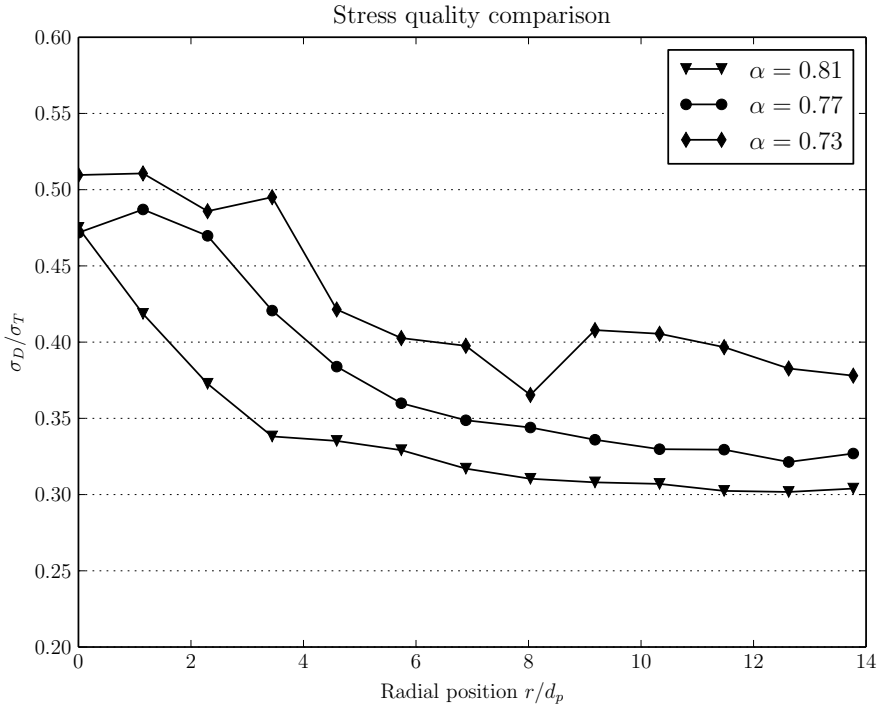

Figure 4.4: The deviatoric fractions for different solid fractions

The deviatoric fraction, or the shear stress, shows a tendency to increase relative to the trace for decreasing solid fractions. The higher the solid fraction, the quicker the data tend to a limit of 0.3, indicating that the shear stresses are absorbed faster by denser systems. The reason for the increase in deviation from a mean curve with decreasing solid fractions is attributed to an increase of importance for high contact forces in rare circumstances. Around 80 samples are used for these curves and for dense systems, each sample is likely to have a lot of particle contacts occurring with significant forces involved. The more dilute the systems become, the less frequent particles contacts become. But there might still be occasions where, for example, some particles lock close to the rotating ring and the forces thereby introduced will be so large that a big impact on the averages will be made.

Qualitatively, the trace of the stress tensor behaves similarly independent of solid fraction but as can be seen in figure 4.5 the magnitude differs a lot. For each solid fraction, σ_T is fairly constant through the entire domain, possibly decreasing some towards the outer parts, but it differs two orders of magnitude between

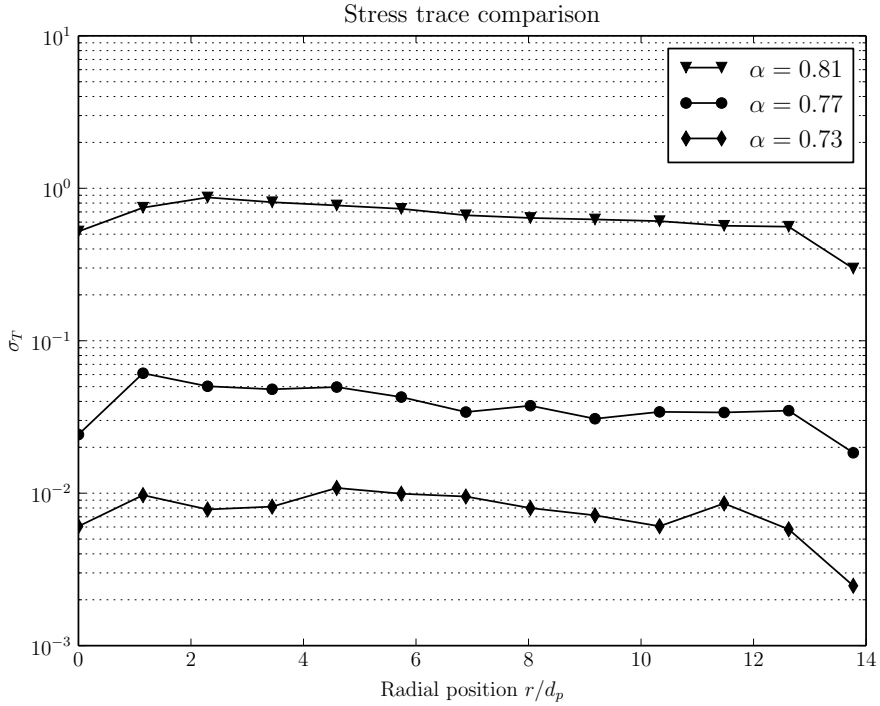

Figure 4.5: The trace of stresses for different solid fractions

the highest and the lowest solid fraction. It is believed that the increase in magnitude for higher α is due to that the trace is a measure of the mean of the normal forces between the particles. Denser system yield more contacts and more force is required to shear the system. This then in turn yield higher stresses.

4.2.2 Influence of friction

The friction between particles affects the magnitude of the tangential forces (eq. 2.4). The lower the friction, the easier the particles will slide against each other and the transfer of forces between particles will decrease. Figures 4.6 and 4.7 shows the stresses for different particle friction coefficients (μ).

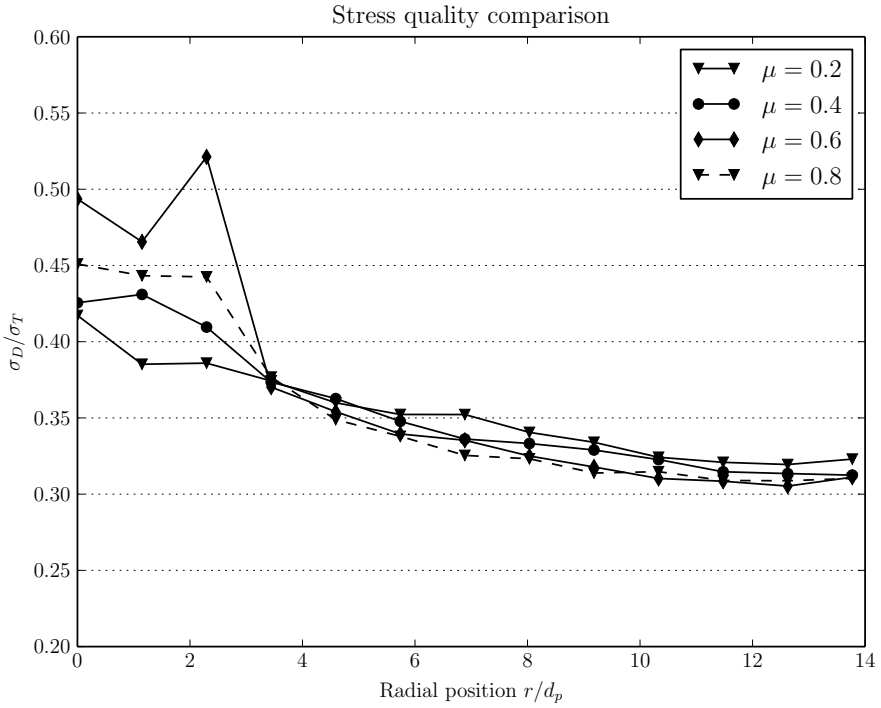

Figure 4.6: The deviatoric fraction for different particle frictions

The deviatoric fraction for different frictions is fairly similar and compared to solid fraction, friction does not seem to have a large impact on σ_D. A general trend is that, for increasing friction, there will be slightly higher stresses close to the inner wall and that they will decay a bit more farther out in the geometry. The trend is not strong and it indicates that the particle friction might not significantly influence the character of the stresses. This result is maybe somewhat contradictory to expectations. It is not difficult to believe that when the particles transfer less tangential forces, the shear stresses would decrease.

From studying the trace it is clear that the particle friction has a big impact on the stress magnitude. For $\mu = 0.6$ and $\mu = 0.8$ the friction seems high enough so that the same forces are transferred in the inner region of the geometry. But they are in lesser degree transferred through the system for $\mu = 0.6$. For $\mu = 0.4$ even less forces seem to propagate in the system, including the inner region, but the cases seem qualitatively similar. For the lowest friction $\mu = 0.2$, the curve does no longer resemble the other cases. It is believed that the friction is now so low that the particles easily slide against each other and the force cannot be transferred into the domain.

The results showing that the particle friction affects the stress magnitude indicates that the particle friction is an important simulation parameter that requires a thorough control over. This especially since low friction suggest a different behavior for the system compared to higher frictions.

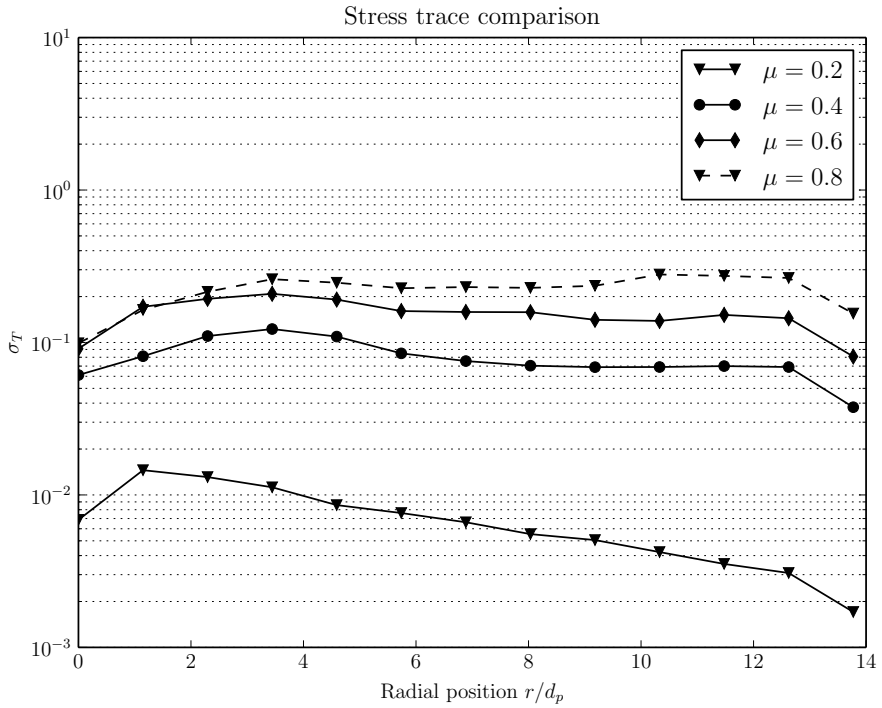

Figure 4.7: The trace of stresses for different particle frictions

4.2.3 Influence of particle size distributions

When particles of the same size are simulated, they will form a crystal structure which can be very stiff and difficult for particles to break loose from. Figure 4.8 shows a comparison between the initial configuration of the particles and the one after 10 simulated seconds for a certain simulation.

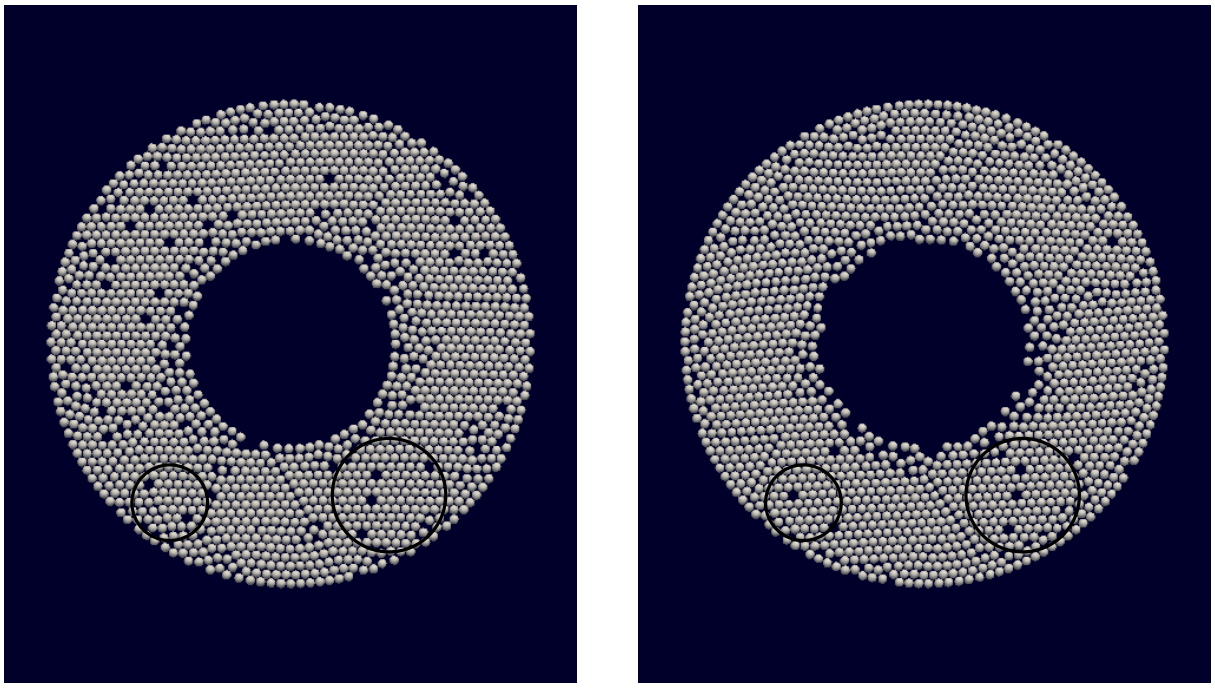

(a) Initial configuration

(b) End configuration

Figure 4.8: Comparison of the initial and the final particle configuration

As highlighted in figure 4.8, some empty spaces remain during the entire simulation that barely move. This is due to the strong structure formed. Some studies use two different particle sizes in order to reduce the tendency for particles to form these crystal structures. The effect of having two different particles sizes compared to just one size has thus been investigated. A comparison of stresses between those cases is shown in figures 4.9 and 4.10.

The deviatoric fraction for both cases (fig. 4.9) seems to agree fairly well close to the outer ring and it is only slightly lower close to the inner ring for the bimodal distribution. But the deviatoric fraction decreases more rapidly in the middle region of the system for the case with two particle sizes. A possible explanation is that in the later case, the particles can move more freely due to the absence of a rigid lattice structure. An easier movement between particles means that less shearing forces would be transferred into the system.

The trace of the stress tensors for both setups follow each other well in the inner regions of the system. From approximately the middle of the geometry, a difference appears where the trace is higher for the simulation with dual particle sizes. This might be physically correct and come as a consequence of the difference in size, but it might also be an error from the simulations. Namely, a probable source of error is the two-dimensional assumption made to evaluate the stress (eq. 3.5). This assumption works well for equally sized particles since the point of contact will be on the same height for all particles. But for particles of different size, since they are represented as spheres, the point of contact between a small and a large particle will be at a different height than that of two equally sized ones. This allows the larger particles to climb above the smaller ones and the smaller particles to even stack on each other (fig. 4.11(a)). To mitigate this problem in the simulations, an artificial force is introduced in the third direction to fixate the particles in that direction. This efficiently forces all particles to lie on a plane (fig. 4.11(b)) but the problem of some particle overlap due to the different sizes still remains. The problem is that it also introduces the uncertainty whether the artificial force affects the simulations. Two simulations with the same settings except for the added force are presented in figures 4.12 and 4.13. The deviatoric fractions coincide well, supporting the conclusion that the results shown in figure 4.9

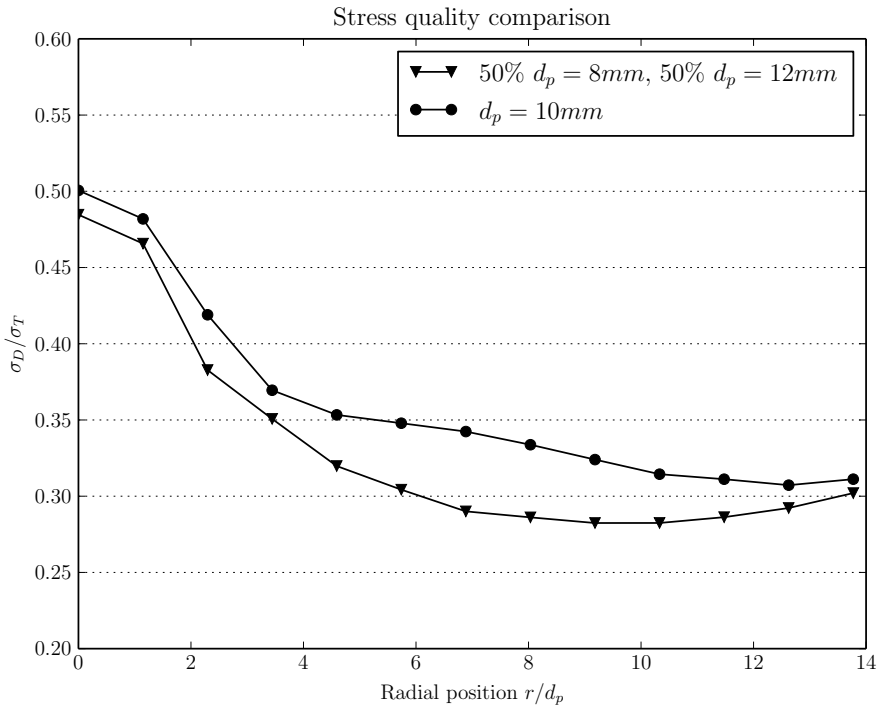

Figure 4.9: The deviatoric fractions for different particle size distributions

are physical. The trace is a bit smaller for the case with artificial forces but the curves otherwise follow each other relatively closely. All together makes this for reason to believe that the deviatoric fraction decreases somewhat in the middle region of the geometry when two particle sizes are used instead of one. The effect of two particle sizes on the magnitude is not as clear but there are indications that the σ_T might be higher.

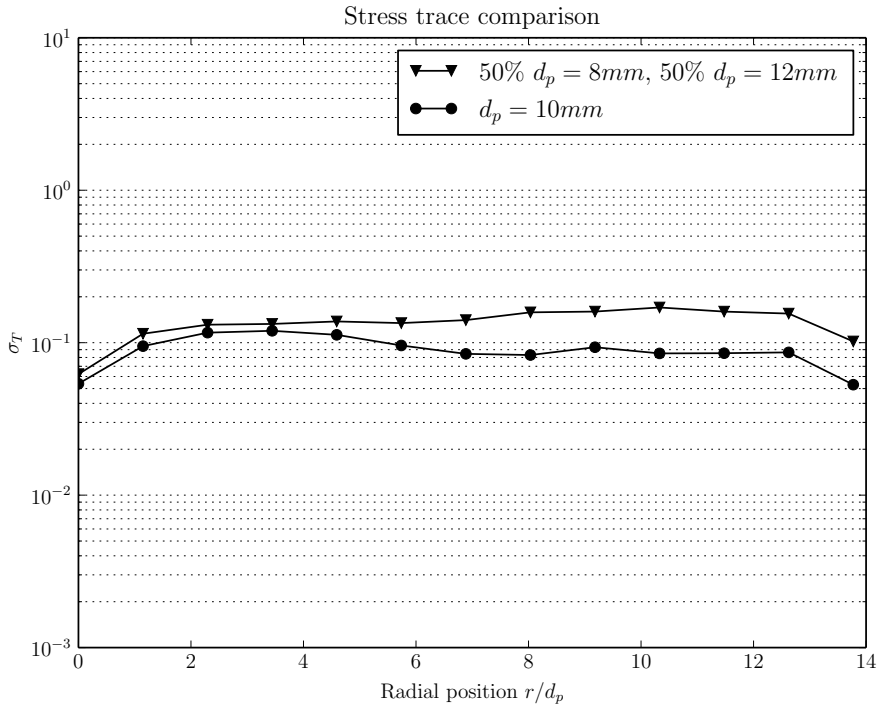

Figure 4.10: The trace of stresses for different particle size distributions

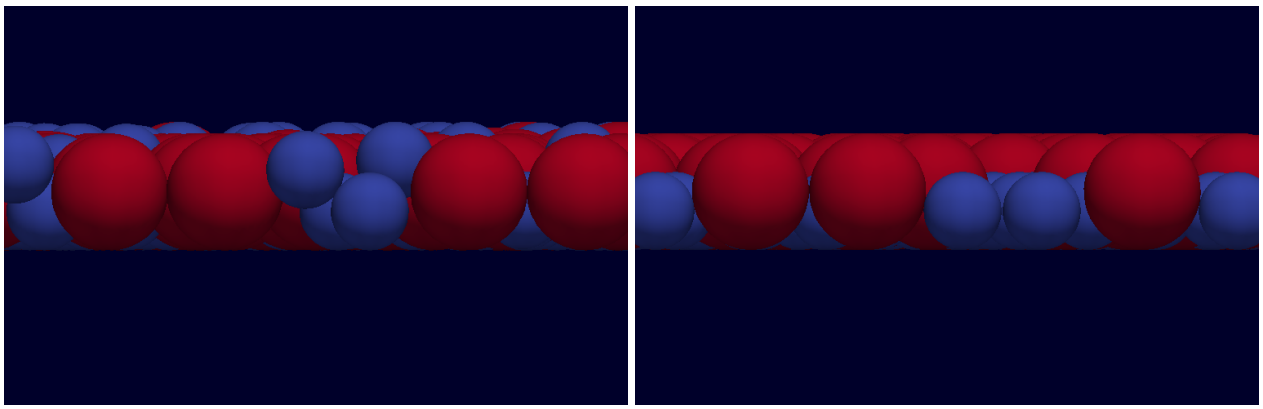

(a) Without artificial force

(b) With artificial force

Figure 4.11: Comparison of particle placement when two particle sizes are used

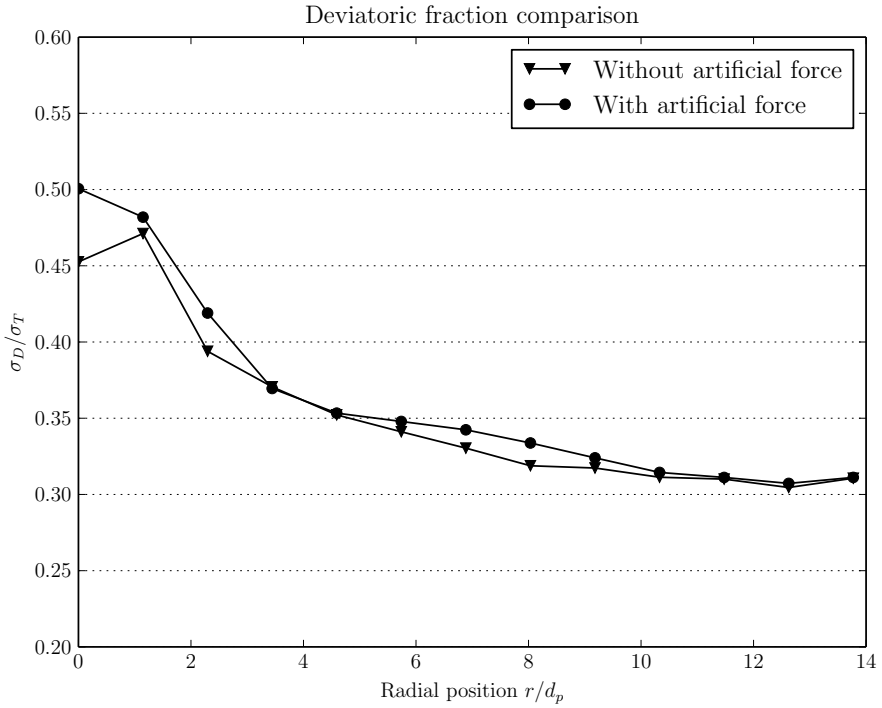

Figure 4.12: The deviatoric fractions with and without artificial force added

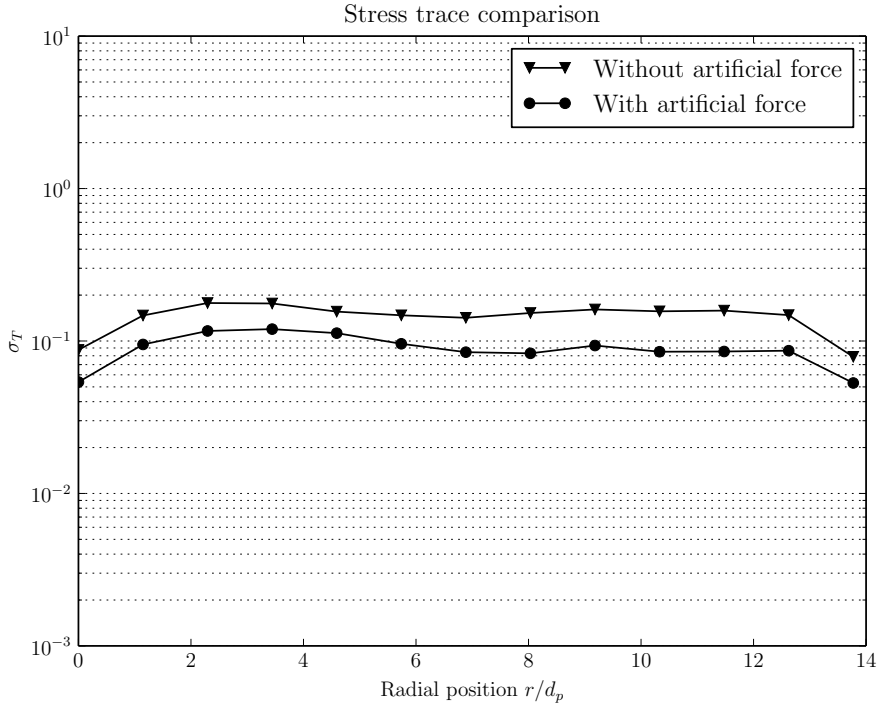

Figure 4.13: The trace of stresses with and without artificial force added

4.3 Influence of shear rate on shear stress

In the introduction (sec. 1.1) it was mentioned that for granular flows, the shear stress is a function of the shear rate. The flows exhibit gas-like regimes for certain shear rates and solid-like for some others. In figure 4.14 system average shear stress as a function of the dimensionless shear rate $\dot{\gamma}$ is shown. Each data point represents a full $10s$ simulation with the corresponding setup (a certain α and a certain rotational frequency). Theoretically [1], there should be for low shear rates be no dependence between the stress and the shear rate. For the high shear rates, the slope n of the stress/shear rate curve should be around $n = 2$ in the log-log diagram.

When analyzing results from the graph, care has to be taken regarding the detail of information. Trends can most likely be trusted while exact relations would probably require more data to ensure the statistics.

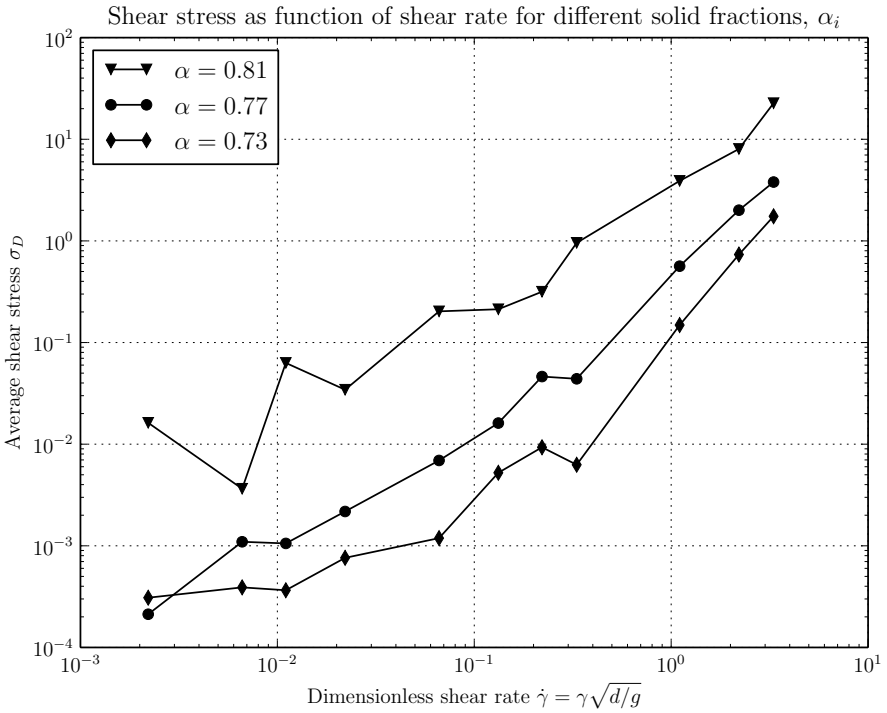

Figure 4.14: Shear stress as function of shear rate

For higher shear rates both simulations for solid fractions $\alpha = 0.73$ and $\alpha = 0.77$ show a dependence such that $n \approx 2$, according to expectations. The data points for the higher end of the shear rates all collapse fairly well on the same line for both solid fractions which increases the credibility of the trend.

When the shear rate decreases, different trends can be seen. For the lowest solid fraction $\alpha = 0.73$, the curve flattens quite a lot and for the lower shear rates the stress seem to be almost independent of the rate. The accuracy of the data is likely lesser than that for the higher shear rates. But it is safe to say that the trend of the graph is clearly flatter in the low shear rates compared to the higher. When the solid fraction somewhat increases, to $\alpha = 0.77$, the clear decrease in dependence seen for the lower solid fraction is no longer visible. The curve flattens some, but not as much as for $\alpha = 0.73$ and a slope around $n \approx 1$ can be seen.

For the case with the highest solid fraction the dependence for the high shear rates is slightly weaker than for the other solid fractions and tends rather to $n \approx 1 - 1.5$. This dependence seem to persist or slightly decrease when the shear rates go down, to the point where the results become inconsistent.

It is believed that, for the highest solid fraction, $\alpha = 0.81$, the lattice structure that the particles formate is difficult to escape, which causes roughly the same behavior independent of the shear rate applied. From the simulation with the highest shear rate a visual inspection shows that the entire mass of particles has a rigid body movement. The high shear rate engages the particles to a degree where the friction of the outer wall is not enough to keep the outer layer still. This is possible since the crystal structure created by the particles

stretches through almost the entire domain. For the lower solid fractions in the high shear rates, the inner region of particles is strongly engaged and the outer region is still in a lattice structure but it does not cover as much of the domain. In such a case, there is a band allowing an intermediate region.

4.4 A word on graph deviations

The simulations are relatively sensitive in relation to spontaneous formation of force chains. In certain simulations one event can impact quite heavily on the calculated stresses. If there is, for some reason, a big spike in forces (fig 4.15), it will be seen in the averaged stresses. This is because the average stress is normally much smaller than the spike. This is especially true for the simulations with a low angular frequency since most of the time the forces in the system are low. There are usually not more than one or two of these spikes during a $10s$ simulation. A simulation time where at least a few similar force spikes would occur would improve the accuracy of the calculations.

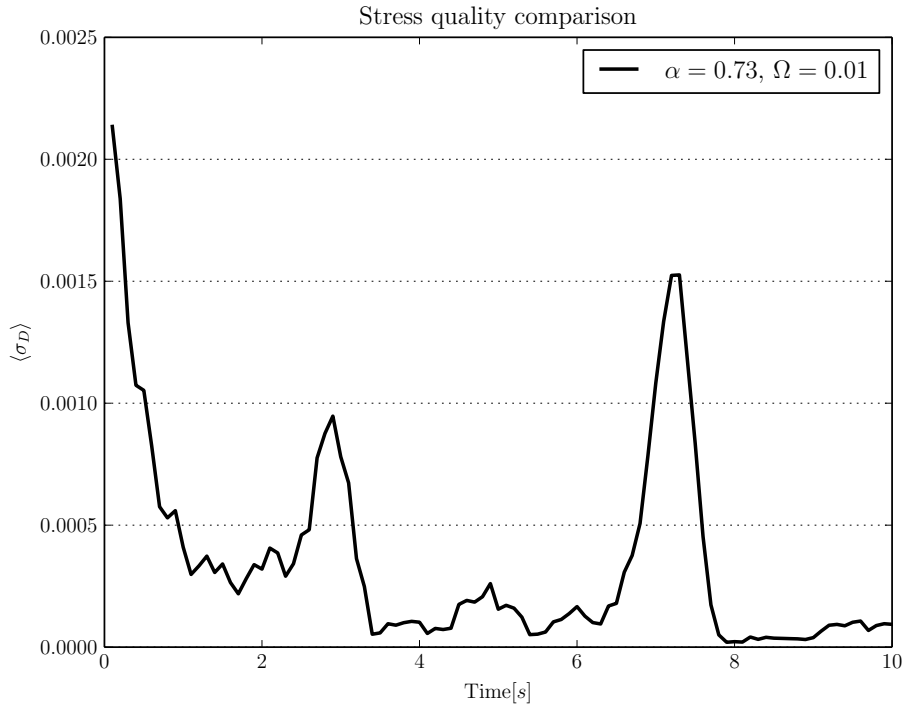

Figure 4.15: Typical spike in stresses

5 Summary and conclusions

This project sets out to investigate how stresses in a dense dry granular flow are influenced by system characteristic properties. A Couette shear cell is used as the test geometry, which allowed for comparisons with the literature and the reuse of existing theory developed for that geometry.

5.1 Methodology

In the study Discrete Element Modeling is used to simulated the system. Each particle is individually treated in a framework where forces on the particle result in motion according to the Newtons second law. A soft-sphere model is used to model particle-particle and particle-wall contacts due to the dense nature of the system. A method for calculating system properties such as stresses is implemented. The geometry is divided into a number of bins where particle stresses is averaged into a bin stresses. This results in a spacial average where stresses become a function of the radial coordinate.

5.2 Results

In general, trends and tendencies have been visible in the results, whereas some specific features have been more difficult to observe. The nature of the problem is such that system averages are very different from instantaneous snapshots.

For the simulations in general has it has been observed that:

- There is an initial time where the system behaves differently compared to the rest of the simulation. This is due to the initial particle setup and care should be taken not to sample data from this period.
- To achieve a dense system, an initial placing of the particles in a triangular lattice yields high solid fractions but also a stiff structure. Either long simulation times or the use of different particle sizes, maybe both, are preferred to ensure independence of the initial setup.
- If two different particles sizes are present, spheres are not appropriate as particles in conjunction with a two dimensional methodology. Cylinders or an adapted theory would be needed since particles will climb on each other.
- For simulations with a single particle size, no problem in using a two dimensional methodology has been encountered but the particles instead formed strong crystal structures.

When evaluating the stress response to different characteristic system properties it is concluded that:

- Studying the solid fraction shows:
  - For increasing the solid fraction the deviatoric fraction conforms to an initial band, close to the inner ring, with higher shear stresses and decreases to an almost constant limit farther out in the system.
  - The solid fraction has a large impact on the magnitude of the stresses with a difference of several orders of magnitude for solid fractions spanning from $\alpha = 0.73$ to $\alpha = 0.81$.
  - Even if the magnitude of the stresses changes a lot for different solid fractions, the stresses remain fairly constant through the system independent of α.
- Studying the particle friction shows:
  - Impact on the deviatoric fraction is small. An increase close to the inner ring can be seen with an increasing friction but rather soon after the inner ring the results coincided well.
  - The magnitude of the stresses is strongly dependent on the friction where the biggest difference between the highest and lowest friction is roughly two orders of magnitude. It is noticeable that for the lowest friction the trace of the stress tensor is no longer constant but decreasing.
- Studying the effect of different particle size distributions shows:

- Stress data from studying setups with more than one particle size are difficult analyze since either the two dimensional assumption is violated or the introduced artificial forces might affect the results.
- The deviatoric fraction is decreased more in the middle region of the device for a bimodal particle distribution than for a single size setup. But the stresses coincide fairly well close to the inner and outer walls.
- The trace of the stress tensor might be higher towards the outer region of the geometry for the setup with two sizes of particles.

- Finally, from studying the impact of the shear rate on the system results shows:
  - The lower the solid fraction, the closer are the results to theoretical expectations. For the lowest sold fraction tested, $\alpha = 0.73$, a shift in trend is clearly visible when the shear rate increases. For the highest solid fraction tested, $\alpha = 0.81$, the same shift in trend is nonexistent.
  - To better map out the shear stress on the shear rate more simulations are needed. It is believed though that a setup in which the particles do not form such strong crystal patterns would benefit the results the most, since for the highest shear rates rigid body motion is observed for the entire mass of particles.

References

[1] Gabriel I. Tardos, Sean McNamara, and Ilkay Talu. Slow and intermediate flow of a frictional bulk powder in the Couette geometry. *Powder Technology* **131** (2003), 23–39.

[2] Marc Lätzel, Stefan Luding, and Hans J. Herrmann. Macroscopic material properties from quasi-static, microscopic simulations of a two-dimensional shear-cell. *Granular Matter* **2** (2000), 123–135.

[3] Daniel W. Howell, R. P. Behringer, and Christian Veje. Stress Fluctuations in a 2D Granular Couette Experiment: A Continuous Transition. *PHYSICAL REVIEW LETTER* (1999).

[4] Martin C. Marinack et al. Couette grain flow experiments: The effects of the coefficient of restitution, global solid fraction and materials. *Powder Technology* **211** (2011), 144–155.

[5] H.P. Zhu et al. Discrete particle simulation of particulate systems: Theoretical developments. *Chemical Engineering Science* (2007).

[6] Edwared Dintwa, Engelbert Tijskens, and Herman Ramon. On the accuracy of the Hertz model to describe the normal contact of soft elastic spheres. *Granular Matter* **10** (2008), 209–221.

[7] Stefan Luding. Objective constitutive relations from DEM (). ISBN-13: 978-3-936310-17-7.

[8] C. T. Veje, Daniel W. Howell, and R. P. Behringer. Kinematics of a two-dimensional granular Couette experiment at the transition to shearing. *PHYSICAL REVIEW E* **59** (1999), 739–745.

[9] S. Luding et al. From discrete element simulations to a continuum model. *Comput. Methods Appl. Mech. Engrg.* **191** (2001), 21–28.

[10] Brian Miller, Corey O'Hern, and R.P Behringer. Stress Fluctuations for Continuously Sheared Granular Materials. *PHYSICAL REVIEW LETTER* **77** (1996).

[11] Steffen Schöllmann. Simulation of a two-dimensional shear cell. *PHYSICAL REVIEW E* **59** (1999).